Chronic BDNF simultaneously inhibits and unmasks superficial dorsal horn neuronal activity

Sascha R.A. Alles[1,2*†], Max A. Odem[3†], Van B. Lu[2,4], Ryan M. Cassidy[5], Peter A. Smith[2*]

[1]Department of Anesthesiology & Critical Care Medicine, University of New Mexico Health Sciences Center, Albuquerque, NM, USA

[2]Neuroscience and Mental Health Institute & Department of Pharmacology, University of Alberta, Edmonton, AB, Canada

[3]Department of Microbiology and Molecular Genetics, McGovern Medical School at UTHealth, Houston, TX, USA

[4]Wellcome-MRC Institute of Metabolic Science, University of Cambridge, UK

[5]Department of Psychiatry and Behavioral Sciences, Vanderbilt University Medical Center, Nashville, TN, USA

[†]authors contributed equally

***Corresponding author:**

Sascha R.A. Alles, PhD

Assistant Professor (research)

Department of Anesthesiology & Critical Care Medicine

MSC 10-6000

2211 Lomas Blvd. NE, ACM 200

University of New Mexico School of Medicine

Albuquerque, NM 87106 USA

Email: salles@salud.unm.edu

Phone: 505-272-7793

Abstract

Brain-derived neurotrophic factor (BDNF) is critically involved in the pathophysiology of chronic pain. However, the mechanisms of BDNF action on specific neuronal populations in the spinal superficial dorsal horn (SDH) requires further study. We used chronic BDNF treatment (200 ng/ml, 5-6 days) of defined-medium, serum-free spinal organotypic cultures to study intracellular calcium ($[Ca2+]_i$) fluctuations. A detailed quantitative analysis of these fluctuations using the Frequency-independent biological signal identification (FIBSI) program revealed that BDNF simultaneously depressed activity in some SDH neurons while it unmasked a particular subpopulation of 'silent' neurons causing them to become spontaneously active. Blockade of gap junctions disinhibited a subpopulation of SDH neurons and reduced BDNF-induced synchrony in BDNF-treated cultures. BDNF reduced neuronal excitability by measuring spontaneous excitatory postsynaptic currents. This was similar to the depressive effect of BDNF on the $[Ca2+]_i$ fluctuations. This study reveals novel regulatory mechanisms of SDH neuronal excitability in response to BDNF.

Introduction

Injury to, or disease of, the somatosensory system frequently generates chronic and sometimes intractable neuropathic pain (1,2). In experimental animals, peripheral nerve damage, such as that generated by chronic constriction or section of the sciatic nerve, induces pain-related behaviours that serve as a model for human neuropathic pain (3,4). Seven or more days of sciatic nerve injury promote an enduring increase in the excitability of first order primary afferent neurons (5–8). These become chronically active and release a variety of mediators (cytokines, chemokines, neuropeptides, ATP and growth factors) that predispose spinal microglia to a more 'activated' state (9–14). These in turn, release further mediators, including brain derived neurotrophic factor (BDNF) that promote a slowly developing, but persistent increase in excitability of second order neurons in the spinal dorsal horn. This 'central sensitization' is thought to be responsible for the allodynia, hyperalgesia, spontaneous pain and causalgia that characterize neuropathic pain (3,15). Spinal actions of BDNF involve alteration in Cl^- gradients such that the normally inhibitory actions of GABA become excitatory (16,17). There is also increased excitatory synaptic drive to putative excitatory neurons (9,18). This results in an overall increase in excitability as monitored by confocal Ca^{2+} imaging in organotypic cultures of rat or mouse spinal cord (9,18–20). Despite this, the long-term effects of upregulated BDNF on neuronal plasticity in the superficial dorsal horn (SDH) are not fully understood.

Naïve cultures display spontaneous oscillatory changes in intracellular Ca^{2+} levels $[Ca2+]_i$ and we have previously shown that the amplitude and frequency of these changes in $[Ca2+]_i$ are profoundly increased following 5-6 d treatment with BDNF (20). We used this model and a new Frequency-independent biological signal identification (FIBSI) (21) program to quantitatively measure the fluctuations of $[Ca2+]_i$ and examine their synchronicity. Unexpectedly, we observed two opposite effects of BDNF that appeared to occur simultaneously. First, BDNF caused an overall decrease in fluctuation size. Second, we noticed a particular population of SDH neurons in naïve cultures that did not display typical, marked fluctuations of $[Ca2+]_i$. This population of 'silent' neurons was absent in BDNF-treated cultures, suggesting that BDNF unmasks these 'silent' neurons and causes them to become spontaneously active. We next investigated the role of gap junctions in mediating the $[Ca2+]_i$ fluctuations; application of the gap junction blocker octanol to chronic BDNF-treated neurons revealed a subpopulation of neurons that generate low-frequency, large $[Ca2+]_i$ fluctuations. Further pharmacological experiments indicated the $[Ca2+]_i$ fluctuations in active neurons are regulated by diverse mechanisms including voltage-gated calcium and sodium channels as well as GABA and NMDA receptors. Finally, we used FIBSI to reanalyze a previous dataset of spontaneous excitatory postsynaptic current (sEPSC) recordings from BDNF-treated dorsal horn neurons in order to qualitatively compare the effects of BDNF on the sEPSCs and $[Ca2+]_i$

fluctuations in SDH neurons. The depressive effects of BDNF on the sEPSCs in delay and tonic-firing SDH neurons were consistent with the effects on the $[Ca2+]_i$ fluctuations. This study reveals novel mechanisms of BDNF regulation of dorsal horn excitability, which has implications for the study of chronic neuropathic pain physiology.

Results

Chronic BDNF treatment of spinal organotypic cultures simultaneously depresses and unmasks $[Ca2+]_i$ fluctuations in superficial dorsal horn neurons

In previous work we identified that chronic BDNF treatment (200 ng/ml, 5-6 days) induces fluctuations compared to naïve cultures (20,22). In this study, we performed a detailed quantitative analysis of the fluctuations in $[Ca2+]_i$ using Fluo-4 AM Ca2+ imaging and the FIBSI analysis program (21) to further establish the nature of BDNF-induced changes in lamina II neurons of the SDH. Refer to **Fig 1A1-A3** for an example of $[Ca2+]_i$ fluctuations detected by the FIBSI program. Inspection of the FIBSI-processed recordings revealed a subset of naïve, untreated neurons were 'silent' (**Fig 1B**, left) for the duration of the recording with notably smaller amplitudes ('silent' = 1.7 ± 0.04 AU; naïve = 53.7 ± 1.6 AU; BDNF = 25.5 ± 0.7 AU). No 'silent' neurons were found in the BDNF treatment group (**Fig 1B**, right). Refer to **Table 1** for detailed statistical information. This stark contrast suggested BDNF may be unmasking, or activating, these 'silent' neurons. We grouped the fluctuations in the 'silent' neurons together for further comparison to the fluctuations in the other active naïve neurons and BDNF-treated neurons. Log-transformed fluctuation amplitudes (**Fig 1C**) and area under the curve (AUC; **Fig 1D**) were larger in the naïve and BDNF conditions compared to 'silent'. Unexpectedly, both measures were significantly decreased in the BDNF condition compared to untreated. A plausible explanation for this effect was that chronic BDNF induced a concomitant enhancement of $[Ca2+]_i$ fluctuations in some neurons and depression in others. Indeed, the effects of BDNF on the relative frequencies (%) for the fluctuation amplitudes (amplitudes were normalized to the largest fluctuation in each neuron) revealed a biphasic effect; frequencies of the smaller- and larger-amplitude fluctuations were greater in the BDNF-treated neurons compared to the naïve and 'silent' neurons (**Fig 1E**). We next compared the mean parameters between neurons in order to control for differences in sampling periods. A <10% maximal fluctuation amplitude cut-off was applied to each neuron to reduce the effects of low-amplitude noise. As expected, nonparametric comparisons indicated that fluctuation amplitude (**Fig 1F**) and AUC (**Fig 1G**) were both greater in the naïve and BDNF-treated neurons compared to the 'silent' neurons, but were not significantly different between naïve and BDNF-treated neurons. Further analysis of the fluctuation kinetics indicated no effect on duration (**Fig 1H**), a modest, but significant decrease in rise time (i.e., peak time is more negative) compared to the 'silent' neurons (**Fig 1I**), and no effect on frequency (**Fig 1J**).

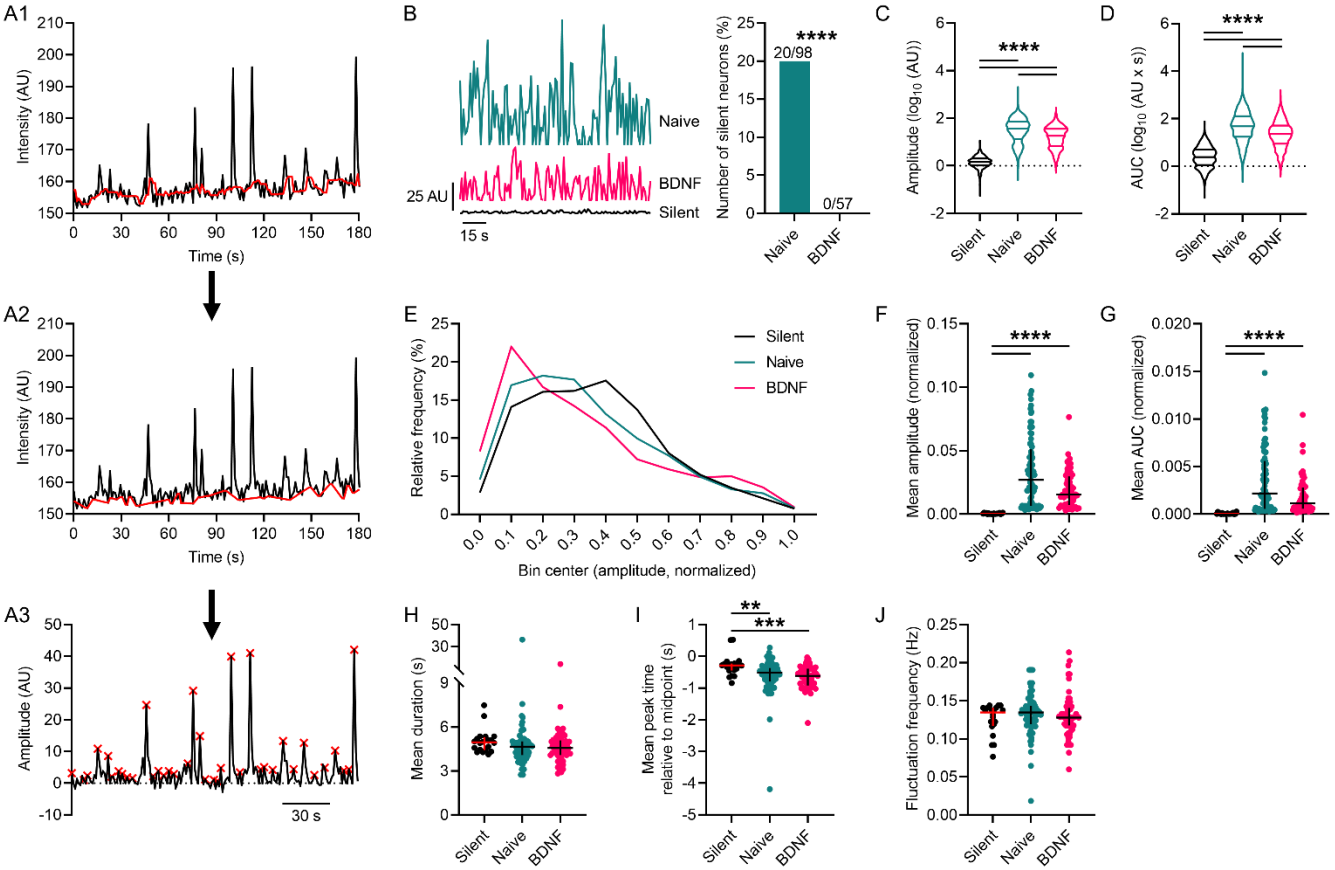

Figure 1. BDNF-induced fluctuations of $[Ca2+]_i$ in superficial dorsal horn neurons. **(A1-A3)** Example recording $[Ca2+]_i$ fluctuations sampled in a SDH neuron and the processing steps used by the FIBSI event-detection program. The running median (red line in A1, window = ~5 s) was calculated based on the raw amplitude (AU) and time coordinate data, then the peaks below the running median were traced to form a reference line (red line in A2), and then the Ramer-Douglas-Peucker algorithm detected waveforms above the reference (red x at event peaks). **(B)** Left: Examples of $[Ca2+]_i$ activity detected by FIBSI in 3 different neurons. Right: The proportion of 'silent' neurons in the BDNF-treatment condition was significantly reduced compared to the naïve condition. Proportions were compared using a Fisher exact test. **(C-D)** Violin plots of the log-transformed values for fluctuation amplitude and AUC. Fluctuation amplitudes and AUC were significantly increased in naïve and BDNF-treated neurons compared to the 'silent' neurons, while both measures in the BDNF-treated neurons were significantly reduced compared to naïve. Neurons sampled: 'silent' n = 20 (849 fluctuations), naïve n = 78 (2651 fluctuations), and BDNF n = 57 (1555 fluctuations). Median with quartiles shown. Comparisons made using Brown-Forsythe and Welch's ANOVA tests and Games-Howell post-hoc test. **(E)** Relative frequency (%) of the fluctuations binned by amplitude. Amplitude values were normalized to the largest fluctuation in each neuron. **(F-G)**

The mean fluctuation amplitude and AUC in the naïve and BDNF-treated neurons were significantly increased compared to the 'silent' neurons. **(H-J)** Further analysis revealed little to no effect of BDNF on fluctuation duration or frequency, but the fluctuations in 'silent' neurons exhibited longer rise times. For scatterplots F-J, the fluctuations that were <10% the maximal fluctuation amplitude in each neuron were omitted to reduce the effects of low-amplitude noise. Scatterplots in F-J show the median with the interquartile range. All comparisons of medians in F-K were made using Kruskal-Wallis tests and Dunn's post-hoc test. $^{**}P < 0.01$, $^{***}P < 0.001$, $^{****}P < 0.0001$.

Figure	Test	Post-hoc comparisons
1B	Fisher exact test Naïve vs BDNF: P < 0.0001	n/a
1C	Brown-Forsythe $F_{(2, 4598)}$ = 3373, P < 0.0001 Welch's ANOVA $W_{(2, 2892)}$ = 5458, P <0.0001	Games-Howell's multiple comparison test Silent vs naïve: P < 0.0001; silent vs BDNF: P < 0.0001; naïve vs BDNF: P < 0.0001
1D	Brown-Forsythe $F_{(2, 4280)}$ = 1737, P < 0.0001 Welch's ANOVA $W_{(2, 2502)}$ = 2032, P <0.0001	Games-Howell's multiple comparison test Silent vs naïve: P < 0.0001; silent vs BDNF: P < 0.0001; naïve vs BDNF: P < 0.0001
1F	Kruskal-Wallis test KW = 54.23, P < 0.0001	Dunn's multiple comparison test Silent vs naïve: P < 0.0001; silent vs BDNF: P < 0.0001; naïve vs BDNF: P = 0.0939
1G	Kruskal-Wallis test KW = 54.35, P < 0.0001	Dunn's multiple comparison test Silent vs naïve: P < 0.0001; silent vs BDNF: P < 0.0001; naïve vs BDNF: P = 0.0732
1H	Kruskal-Wallis test KW = 4.507, P = 0.1051	n/a
1I	Kruskal-Wallis test KW = 15.04, P = 0.0005	Dunn's multiple comparison test Silent vs naïve: P = 0.0087; silent vs BDNF: P = 0.0003; naïve vs BDNF: P = 0.4002
1J	Kruskal-Wallis test KW = 2.810, P = 0.2454	n/a
2B	Two-way RM ANOVA Interaction: $F_{(1, 77)}$ = 29.27, P < 0.0001, 10.65% total variation Group effect: $F_{(1, 77)}$ = 0.0392, P = 0.8437, 0.028% total variation Treatment effect: $F_{(1, 77)}$ = 14.31, P = 0.0003, 5.208% total variation Subjects (matching) effect: $F_{(77, 77)}$ = 1.994, P = 0.0014, 55.89% total variation	Sidak's multiple comparison test Control vs octanol (Decrease): P = 0.4469; Control vs octanol (Increase): P < 0.0001
2C	Two-way RM ANOVA Interaction: $F_{(1, 77)}$ = 13.95, P = 0.0004, 7.126% total variation Group effect: $F_{(1, 77)}$ = 7.287, P = 0.0085, 4.105% total variation Treatment effect: $F_{(1, 77)}$ = 11.50, P = 0.0011, 5.875% total variation Subjects (matching) effect: $F_{(77, 77)}$ = 1.102, P = 0.3349, 43.38% total variation	Sidak's multiple comparison test Control vs octanol (Decrease): P = 0.9638; Control vs octanol (Increase): P < 0.0001
2D	Two-way RM ANOVA Interaction: $F_{(1, 77)}$ = 13.63, P = 0.0004, 7.764% total variation Group effect: $F_{(1, 77)}$ = 0.080, P = 0.7780, 0.049% total variation Treatment effect: $F_{(1, 77)}$ = 1.725, P = 0.1929, 0.983% total variation Subjects (matching) effect: $F_{(77, 77)}$ = 1.078, P = 0.3709, 47.28% total variation	Sidak's multiple comparison test Control vs octanol (Decrease): P = 0.1876; Control vs octanol (Increase): P = 0.0013
3B	Mann-Whitney test U = 606.5, P = 0.0010	n/a
3C1	Wilcoxon matched-pairs signed rank test W = -1373, P < 0.0001	n/a
3C2	Two-way RM ANOVA Interaction: $F_{(1, 58)}$ = 37.70, P < 0.0001, 6.086% total variation Group effect: $F_{(1, 58)}$ = 38.23, P < 0.0001, 29.22% total variation Treatment effect: $F_{(1, 58)}$ = 83.93, P < 0.0001, 13.55% total variation Subjects (matching) effect: $F_{(58, 58)}$ = 4.736, P < 0.0001, 44.34% total variation	Sidak's multiple comparison test Control vs octanol (Decrease): P < 0.0001; Control vs octanol (Increase): P = 0.0450
4A-B	Paired t tests Control vs 0 Ca^{2+}: Amplitude P > 0.05; Frequency P > 0.05 Control vs Cd^{2+}: Amplitude P > 0.05; Frequency P > 0.05 Control vs Ni^{2+}: Amplitude P > 0.05; Frequency P < 0.001 Control vs nitrendipine: Amplitude P > 0.05; Frequency P < 0.001 Control vs ω-conotoxin: Amplitude P > 0.05; Frequency P < 0.001 Control vs TTX: Amplitude P > 0.05; Frequency P > 0.05 Control vs riluzole: Amplitude P > 0.05; Frequency P < 0.001 Control vs NBQX: Amplitude P > 0.05; Frequency P > 0.05 Control vs D-AP5: Amplitude P < 0.001; Frequency P > 0.05 Control vs kynurenic acid: Amplitude P > 0.05; Frequency P > 0.05 Control vs GABA: Amplitude P > 0.05; Frequency P > 0.05	n/a
5C2	Brown-Forsythe $F_{(3, 2916)}$ = 311.1, P < 0.0001 Welch's ANOVA $W_{(3, 2862)}$ = 504.2, P <0.0001	Games-Howell's multiple comparison test Control vs BDNF (Delay): P = 0.4264; Control vs BDNF (Tonic): P < 0.0001
5D2	Brown-Forsythe $F_{(3, 1761)}$ = 419.3, P < 0.0001 Welch's ANOVA $W_{(3, 2791)}$ = 541.8, P <0.0001	Games-Howell's multiple comparison test Control vs BDNF (Delay): P < 0.0001; Control vs BDNF (Tonic): P < 0.0001
5E2	Brown-Forsythe $F_{(3, 2550)}$ = 159.1, P < 0.0001 Welch's ANOVA $W_{(3, 2759)}$ = 162.3, P <0.0001	Games-Howell's multiple comparison test Control vs BDNF (Delay): P < 0.0001; Control vs BDNF (Tonic): P = 0.0012
5F2	Brown-Forsythe $F_{(3, 2027)}$ = 14.5, P < 0.0001 Welch's ANOVA $W_{(3, 2860)}$ = 27.93, P <0.0001	Games-Howell's multiple comparison test Control vs BDNF (Delay): P = 0.1284; Control vs BDNF (Tonic): P < 0.0001
S3A2	Brown-Forsythe $F_{(3, 71793)}$ = 1122, P < 0.0001 Welch's ANOVA $W_{(3, 54420)}$ = 2011, P <0.0001	Games-Howell's multiple comparison test Control vs BDNF (Delay): P < 0.0001; Control vs BDNF (Tonic): P < 0.0001
S3A4	Brown-Forsythe $F_{(3, 29988)}$ = 851.4, P < 0.0001 Welch's ANOVA $W_{(3, 18137)}$ = 2294, P <0.0001	Games-Howell's multiple comparison test Control vs BDNF (Delay): P < 0.0001; Control vs BDNF (Tonic): P < 0.0001
S3B2	Brown-Forsythe $F_{(3, 55836)}$ = 870.5, P < 0.0001 Welch's ANOVA $W_{(3, 54028)}$ = 850.3, P <0.0001	Games-Howell's multiple comparison test Control vs BDNF (Delay): P < 0.0001; Control vs BDNF (Tonic): P < 0.0001
S3B4	Brown-Forsythe $F_{(3, 22611)}$ = 438.9, P < 0.0001 Welch's ANOVA $W_{(3, 17636)}$ = 1298, P <0.0001	Games-Howell's multiple comparison test Control vs BDNF (Delay): P < 0.0001; Control vs BDNF (Tonic): P < 0.0001
S3C2	Brown-Forsythe $F_{(3, 72912)}$ = 203.0, P < 0.0001 Welch's ANOVA $W_{(3, 51340)}$ = 169.4, P <0.0001	Games-Howell's multiple comparison test Control vs BDNF (Delay): P < 0.0001; Control vs BDNF (Tonic): P < 0.0001
S3C4	Brown-Forsythe $F_{(3, 26038)}$ = 26.33, P < 0.0001 Welch's ANOVA $W_{(3, 14707)}$ = 27.89, P <0.0001	Games-Howell's multiple comparison test Control vs BDNF (Delay): P = 0.0062; Control vs BDNF (Tonic): P = 0.6416
S3D2	Brown-Forsythe $F_{(3, 76383)}$ = 171.1, P < 0.0001 Welch's ANOVA $W_{(3, 51987)}$ = 167.3, P <0.0001	Games-Howell's multiple comparison test Control vs BDNF (Delay): P < 0.0001; Control vs BDNF (Tonic): P < 0.0001
S3D4	Brown-Forsythe $F_{(3, 26111)}$ = 62.09, P < 0.0001 Welch's ANOVA $W_{(3, 16008)}$ = 62.78, P <0.0001	Games-Howell's multiple comparison test Control vs BDNF (Delay): P < 0.0001; Control vs BDNF (Tonic): P < 0.0001

Table 1. Detailed results of statistical analysis per figure.

Octanol, a gap junction blocker, disinhibits a population of superficial dorsal horn neurons in BDNF-treated cultures

It has been shown that gap junctions have regulatory control over network activity in the *substantia gelatinosa* (23–26). Therefore, gap junctions may play a role in regulating the properties of $[Ca2+]_i$ across the network, but the response of individual neurons to the chronic BDNF in the culture may be masked by the complex responses of the different types of neurons to BDNF (20,27). To address this and determine the potential role of gap junctions in mediating the BDNF-induced fluctuations, we recorded $[Ca2+]_i$ from SDH neurons exposed to chronic BDNF and then applied a non-specific gap junction blocker octanol at 1mM for ≥3 min. We again performed a detailed analysis using the FIBSI program and a <10% maximal fluctuation amplitude cut-off was applied to each neuron. Inspection of the FIBSI-processed recordings revealed octanol disproportionately affected some neurons compared to others (i.e., large increases in amplitude and AUC in some neurons vs minor decreases in others). Neurons were grouped based on whether the octanol treatment caused a negative (decrease, n = 39) or positive (increase, n = 40) fold change in mean fluctuation amplitude compared to the BDNF (control) condition (**Fig 2A**). Paired analyses indicated blocking gap junctions with octanol decreased the frequency of the BDNF-induced fluctuations (**Fig 2B**) while increasing their duration (**Fig 2C**) only in the neurons that had a positive fold change in mean fluctuation amplitude. Fluctuation rise time was also significantly decreased in the same group of neurons (**Fig 2D**). These data suggest that blocking gap junctions with octanol selectively disinhibited the response to chronic BDNF in a subpopulation of SDH neurons.

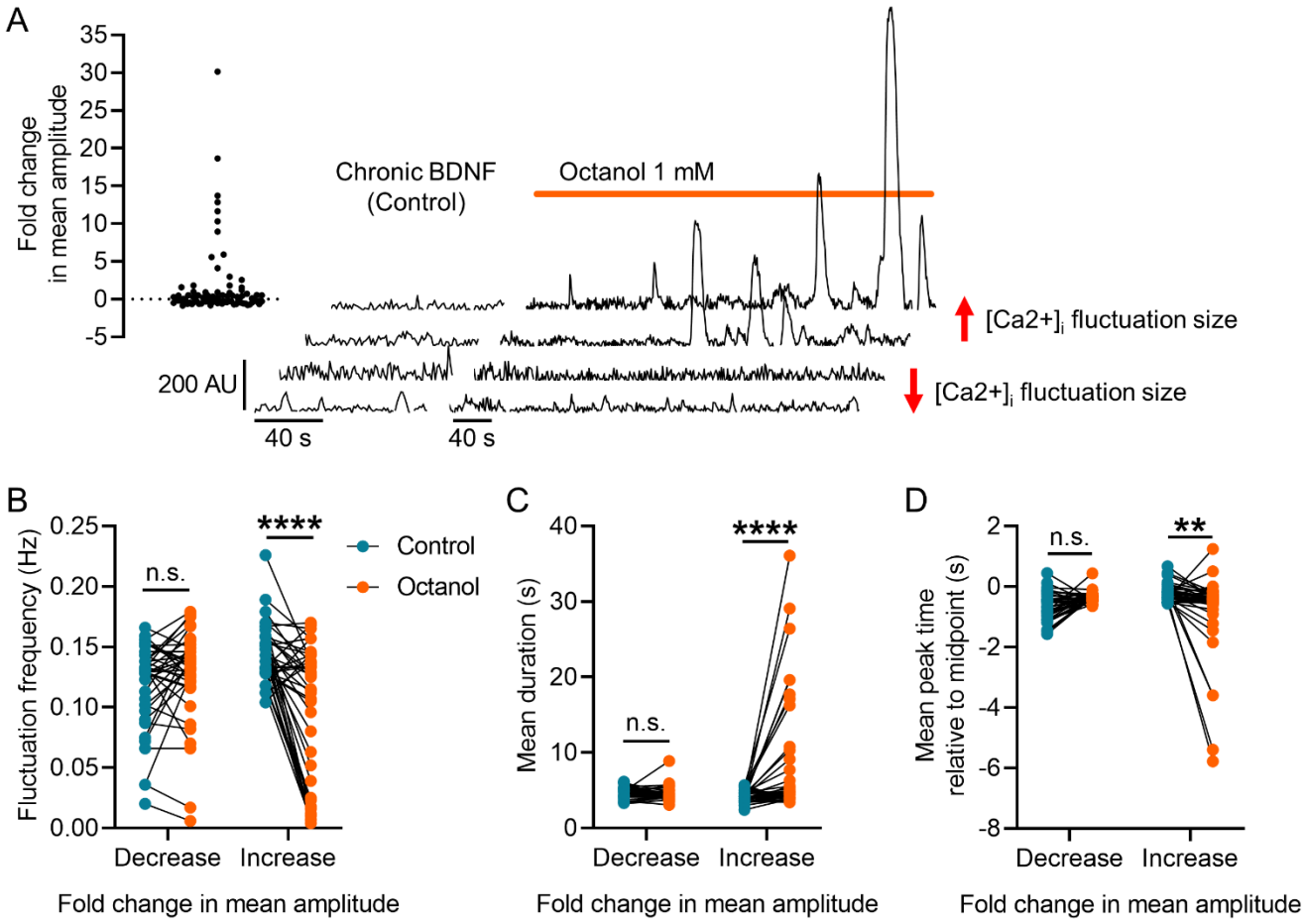

Figure 2. Effect of gap junction blocker octanol on BDNF-induced $[Ca2+]_i$ fluctuations. **(A)** Scatterplot summarizing the effects of octanol on mean fluctuation amplitude and examples of FIBSI-processed recordings. The two bottom recordings show a decrease in fluctuation amplitude and the two top show an increase. **(B-D)** Neurons were sorted based on whether they exhibited a positive or negative fold change in mean fluctuation amplitude in response to octanol. Paired analyses showed octanol selectively and significantly decreased the mean fluctuation frequency, increased the mean fluctuation duration, and decreased the mean fluctuation rise time (i.e., more negative peak time) in the neurons with positive fold changes in mean fluctuation amplitude. Control vs octanol paired comparisons for the groups in B-D were made using two-way repeated measures ANOVAs and Sidak's post-hoc test. $^{**}P < 0.01$, $^{****}P < 0.0001$.

Chronic BDNF induces synchrony of $[Ca2+]_i$ fluctuations in organotypic cultures, and blocking gap junctions reduces BDNF-induced synchrony

Previous work has shown BDNF-treated SDH neurons generate synchronous $[Ca2+]_i$ fluctuations (20). We verified that finding by using the FIBSI-processed recordings and comparing the degree of synchrony

between neurons imaged together in naïve and BDNF-treated cultures. Adjacency matrixes were generated using Pearson *r* coefficients; the recording of each neuron was correlated with every other neuron imaged within the same naïve or BDNF-treated culture using a Pearson correlation matrix. The adjacency matrixes for the BDNF-treated cultures showed the neurons were more positively correlated with Pearson *r* coefficients closer to 1 (**Fig 3A**), suggesting they exhibited more synchronous $[Ca2+]_i$ fluctuations than the naïve cultures. To confirm this prediction, the mean coefficient for each neuron was calculated (i.e., the mean correlation of each neuron with every other neuron in its respective culture; refer to Fig 3A for Fisher Z transformation steps). Comparison of the mean Pearson *r* coefficients revealed BDNF-treated neurons were more positively correlated with other neurons in the culture than naïve neurons (**Fig 3B**). Considering the role gap junctions may play in regulating network activity and synchronous activity, this result led us to anticipate that blocking gap junctions may reduce BDNF-induced synchrony within the culture. We used the same approach to measure synchrony among neurons within the same cultures treated with BDNF prior to application of octanol, and then we asked whether blocking gap junctions caused a decrease in the mean Pearson *r* coefficients. Indeed, octanol caused a net decrease in the mean Pearson *r* coefficient (**Fig 3C1-2**). Closer inspection revealed octanol decreased the mean Pearson *r* coefficient in 100% (25/25) of the neurons in the group with decreased fluctuation amplitudes, while only 63% (22/35) of the neurons in the group with increased fluctuation amplitudes exhibited a decreased mean Pearson *r* coefficient. This suggests that blocking gap junctions may actually increase $[Ca2+]_i$ fluctuation synchrony in some neurons.

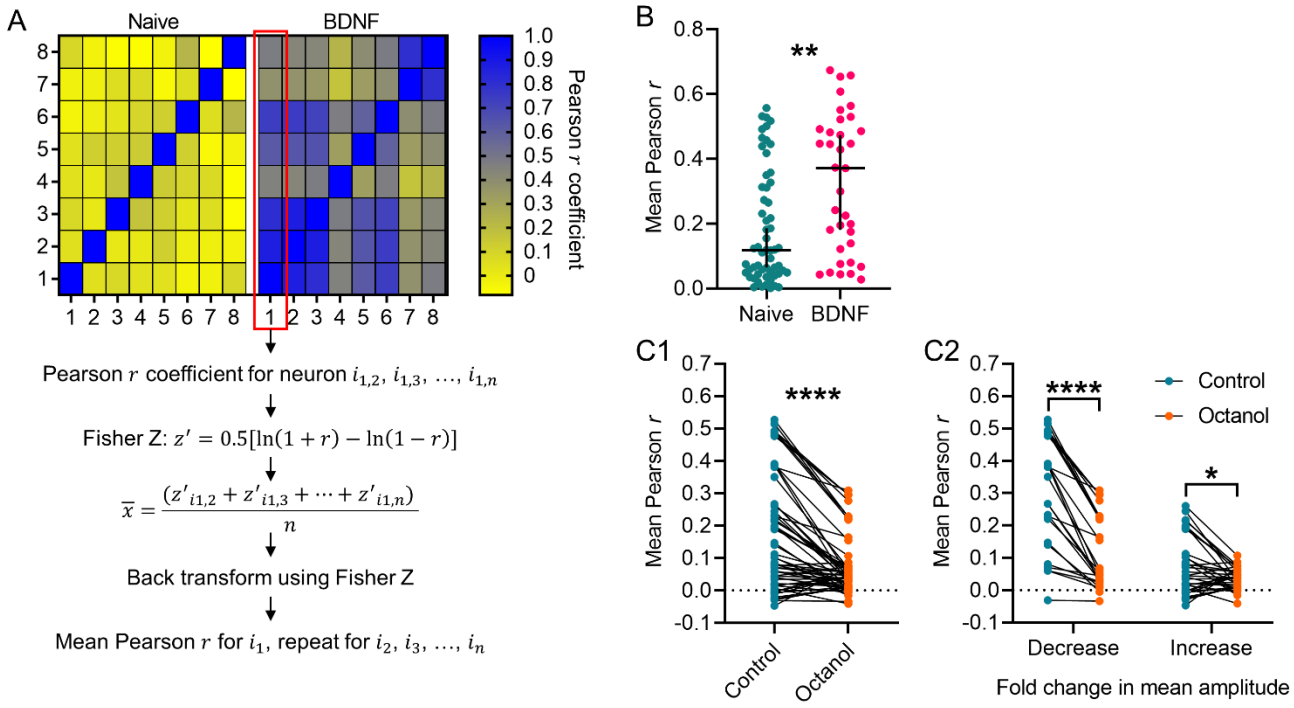

Figure 3. Synchrony of $[Ca2+]_i$ fluctuations in BDNF-treated cultures and the effect of octanol. **(A)** Example adjacency matrix constructed from Pearson *r* coefficients corresponding to the correlation in activity between neurons in a naïve or BDNF-treated culture, each with 8 sampled neurons. Steps to calculate the mean Pearson *r* for each neuron within a culture using the Fisher Z transformation are also depicted. **(B)** Neurons sampled from BDNF-treated cultures exhibited significantly greater mean Pearson *r* coefficients compared to neurons sampled from naïve cultures. Neurons were imaged from 4 naïve cultures and 3 BDNF-treated cultures, each with ≥8 neurons imaged. Medians shown with the 95% confidence interval. Medians were compared using a Mann-Whitney test. **(C1-C2)** Treatment with octanol significantly decreased the mean Pearson *r* in neurons sampled from cultures exposed to chronic BDNF, and this treatment effect impacted both subsets of neurons binned based on their initial response to octanol. Neurons were imaged from 4 cultures. The control vs octanol paired comparison in C1 was made using a Wilcoxon rank sum test. Control vs octanol paired comparisons for the groups in C2 were made using a measures two-way repeated measures ANOVA and Sidak's post-hoc test. $*P < 0.05$, $**P < 0.01$, $****P < 0.0001$.

Pharmacology of $[Ca2+]_i$ fluctuations in BDNF-treated slices

In order to further characterize the properties of the $[Ca2+]_i$ fluctuations, we used pharmacological treatments to block a variety of voltage-gated ion channels, glutamate receptors, and GABA receptors. Comparisons between the pharmacologically-treated neurons and the BDNF-treated (control) neurons revealed the $[Ca2+]_i$ fluctuation amplitudes (**Fig 4A**) and frequency (**Fig 4B**) are controlled by diverse mechanisms (example recordings and data available in **Supplemental Figure 1**). The fluctuations were ablated when extracellular Ca2+ was removed, when all voltage-gated calcium channels (VGCCs) were blocked with Cd2+, when all TTX-sensitive voltage-gated sodium channels (VGSCs) were blocked with tetrodotoxin (TTX), when AMPA or kainite glutamate receptors were blocked, and when GABA was applied to the cultures. Interestingly, the fluctuations remained when we blocked T-type (with Ni2+), L-type (with nitrendipine), or N-type (with ω-conotoxin) Ca2+ channels, although the frequency was significantly reduced with no effect on amplitude. Riluzole, which blocks glutamate release and VGSCs, only affected the fluctuation frequency but not amplitude. Finally, the NMDA blocker D-AP5 was the only blocker to significantly reduce fluctuation amplitudes, but it had no effect on frequency. These data suggest the BDNF-induced $[Ca2+]_i$ fluctuations are controlled by a combination of VGCCs, TTX-sensitive VGSCs, GABA and NMDA receptors.

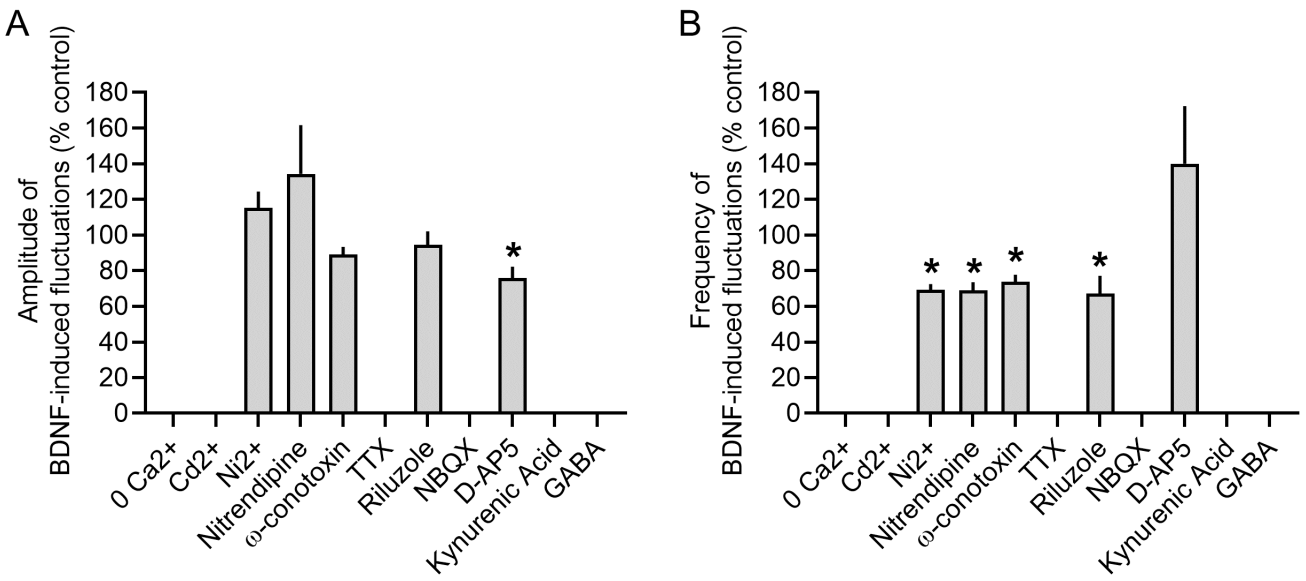

Figure 4. Pharmacology of $[Ca2+]_i$ fluctuations from BDNF-treated cultures. Summary of the effects of various pharmacological treatments on the **(A)** amplitude and **(B)** frequency of the $[Ca2+]_i$ fluctuations in BDNF-treated cultures compared to before drug treatment. Bars show the mean + standard error of the mean. *P < 0.001, paired t-test, n = 5-20 cells per condition.

Clustering spontaneous excitatory postsynaptic currents (sEPSCs) reveals chronic BDNF treatment depresses excitability of delay and tonic-firing superficial dorsal horn neurons, mirroring the effect of BDNF on $[Ca2+]_i$ fluctuations

It is well established that BDNF release in the SDH is involved in neuropathic pain (10,16,17). However, to our knowledge our findings are the first to show chronic BDNF treatment unmasks $[Ca2+]_i$ fluctuations in a subpopulation of SDH neurons while depressing activity in others. We had previously shown that sEPSCs recorded from SDH neurons are perturbed in BDNF-treated spinal cord organotypic cultures (20). It is plausible that the newly discovered unmasked BDNF-induced $[Ca2+]_i$ fluctuations underlie changes in network excitability. We decided to readdress the effects of BDNF on network excitability by using the FIBSI program to quantitatively analyze a previous subset of sEPSC recordings in delay and tonic-firing SDH neurons (example recordings and low-pass filtering/matching methods are available in **Supplemental Figure 2**). Inspection of the sEPSC interevent interval data indicated there might be natural clustering between single “small” sEPSCs and larger summated sEPSCs. We used partitioning around medoids (a medoid is like a centroid, but is restricted to an actual observation in the dataset) to cluster the sEPSCs in each neuron based on 3 sEPSC parameters: interevent interval (ms), amplitude (pA), and charge transfer (Q; essentially area under the curve). Optimal clustering (k medoids = 3-5 per

neuron) identified 3 main clusters of sEPSCs that were present in all delay (**Fig 5A1-A2**) and tonic (**Fig 5B1-B2**) neurons in both control and BDNF treatment conditions (clusters named based on amplitude; interevent interval): 1) small; short, 2) small; long, and 3) large. Two other clusters were identified (small; mid and medium), but they were not present in all neurons or treatment conditions and were not analyzed for this study. We were mainly interested in the effects of BDNF on the cluster of large-amplitude sEPSCs in both neuron types (refer to **Supplemental Figure 3** for the "small" sEPSC analysis). Chronic BDNF treatment significantly decreased sEPSC amplitudes (**Fig 5C1-C2**) and charge transfer (**Fig 5D1-D2**) in the tonic-firing neurons. We did not observe a significant effect on sEPSC amplitudes in the delay neurons, but charge transfer was significantly decreased. The sEPSCs in the BDNF-treated delay neurons were narrower (control duration = 83.6 ± 1.2 ms; BDNF duration = 49.9 ± 0.4 ms). The sEPSC interevent intervals were significantly shorter in both neuron types (**Fig 5E1-E2**), and peak time measurements indicated BDNF significantly increased activation of the sEPSCs in the tonic neuron (**Fig 5F1-F2**).

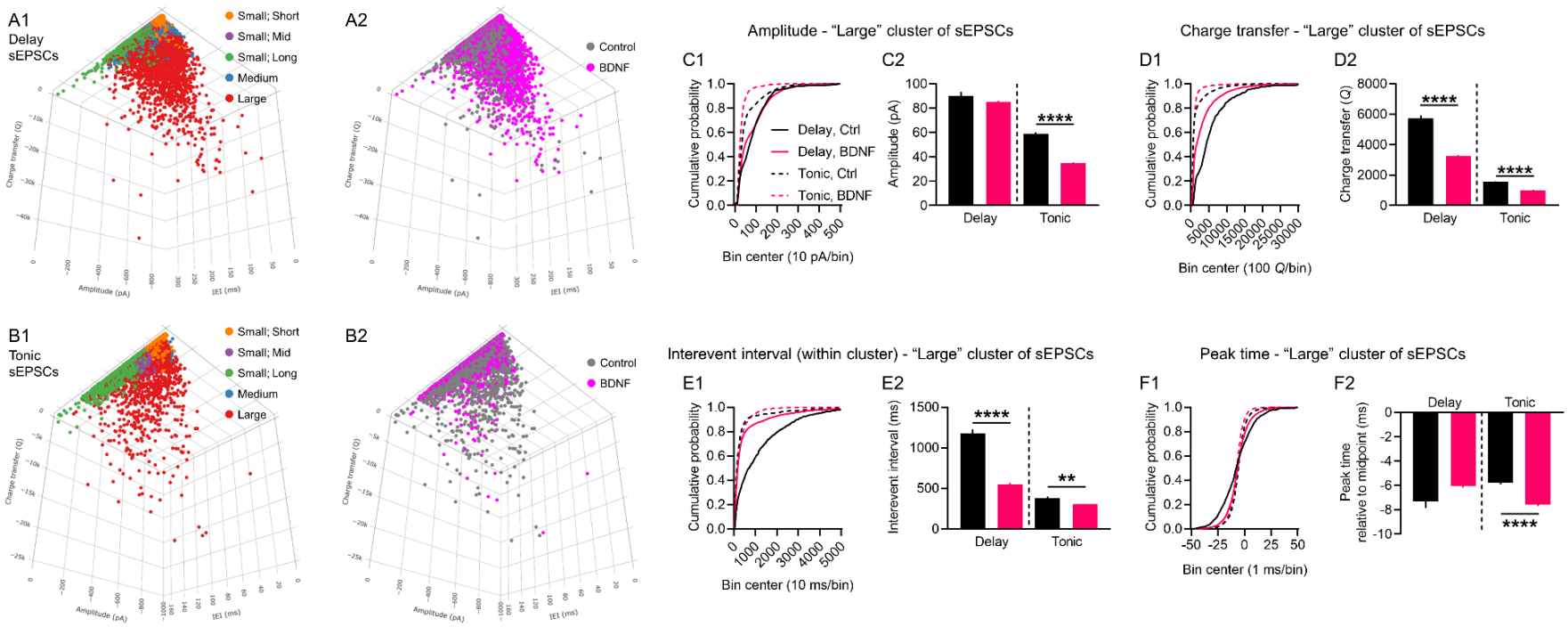

Figure 5. Cluster analysis of spontaneous EPSCs in delay and tonic-firing superficial dorsal horn neurons. Three dimensional representations of the sEPSCs in **(A1-A2)** delay neurons and **(B1-B2)** tonic neurons plotted based on interevent interval (x-axis), amplitude (y-axis), and charge transfer (z-axis). Mapping of the clustering results and treatment shown for the total sample of sEPSCs. The sEPSCs in each neuron were clustered independently from the other neurons. Optimal partitioning around medoids identified 3 primary clusters present in all neurons in both treatment conditions (naming based on amplitude; interevent interval): small; short, small; long, and large. Two additional clusters were identified in some neurons, but were not present in all neurons in both conditions: small; mid and medium. Neurons sampled: 19 delay (5 control, 14 BDNF); 9 tonic (5 control, 4 BDNF). Total number of sEPSCs: 33,206 in delay, control; 108261 in delay, BDNF; 40658 in tonic, control; 36521 in tonic, BDNF. The effects of BDNF on sEPSC amplitude, charge transfer (i.e., area under the curve), and peak time were assessed for the 3 primary clusters (large cluster shown, refer to Supplemental Figure 3 for the two small-amplitude clusters). **(C1-C2)** Treatment with BDNF significantly decreased sEPSC amplitudes in tonic neurons, but a significant effect was not observed in the delay neurons. Cumulative distributions of the measured amplitudes

shown (left) alongside the means ± standard error of the means (right). **(D1-D2)** The BDNF treatment significantly reduced sEPSC charge transfer measures in both delay and tonic neurons. **(E1-E2)** Interevent intervals for the sEPSCs within the large cluster were significantly decreased in the BDNF-treated neurons. **(F1-F2)** The sEPSC activation kinetics were significantly faster in the BDNF-treated neurons, but no significant effect was observed for the sEPSCs in the delay neurons. Large sEPSC cluster sample sizes: delay neurons control n = 753, BDNF n = 4539; tonic neurons control n = 2348, BDNF n = 2367. Comparisons between means were made using Brown-Forsythe and Welch's ANOVA tests and Games-Howell post-hoc test. $^{**}P < 0.01$, $^{****}P < 0.0001$.

Discussion

The present study was undertaken to better understand mechanisms underlying synchronous activity among SDH neurons and the influence BDNF may have on network excitability in naïve, uninjured organotypic cultures. Our experiments indicate long-term exposure to BDNF produces a complex set of neuron-dependent changes in network excitability in the SDH. First, BDNF causes a concomitant activation of Ca2+ signaling in a subpopulation of 'silent' SDH neurons (~20% sampled) and depression of Ca2+ signaling in many others. This finding was largely unexpected as we have previously shown chronic BDNF increases the size and frequency of $[Ca2+]_i$ fluctuations (20). It is plausible that the presence of the 'silent' neurons can greatly influence data analysis and interpretation depending on how they are grouped together, or discarded. Another possibility is that resolution differences between the two event-detection programs used (FIBSI in the current study, Mini Analysis Software (Synaptosoft, NJ)) in the previous study) could influence analysis of the $[Ca2+]_i$ fluctuations. However, the goal of the present study was not to compare/contrast the two programs. The second significant finding was that gap junction signaling may play a crucial role in regulating BDNF-induced changes in Ca2+ signaling in the SDH. Blockade of gap junctions with octanol unveiled a subpopulation of neurons that respond to BDNF with large-amplitude, low-frequency $[Ca2+]_i$ fluctuations. This finding suggests that gap junctions modulate global network activity, either by directly or indirectly inhibiting those particular neurons with increased Ca2+ signaling. Indeed, this is supported by the third major finding that BDNF profoundly increases synchrony of the $[Ca2+]_i$ fluctuations, and blocking gap junctions with octanol reverses BDNF-induced synchrony.

While the physiological correlates of the BDNF-related $[Ca2+]_i$ fluctuations are unclear, we do not think they are being driven by delay or tonic-firing neurons in the SDH. Unlike our analysis of the $[Ca2+]_i$ fluctuations where we describe the 'silent' neurons, we did not observe any unmasking effect(s) of BDNF

on the sEPSCs in the delay or tonic neurons. All neurons sampled in the control (naïve) condition generated visually appreciable, large-amplitude sEPSCs. The main depressive effect of BDNF on the sEPSCs (refer also to **Supplemental Figure 3**) mirrored the main effect of BDNF on comparable properties for the $[Ca2+]_i$ fluctuations. A summary of each dataset (**Fig 6**, table) shows BDNF reduced the amplitude and area under the curve parameters for the $[Ca2+]_i$ fluctuations and large sEPSCs. More nuanced effects were observed for frequency (reciprocal of interevent interval) and activation kinetics: BDNF increased the frequency of the large sEPSCs but had little to no effect on the frequency of the $[Ca2+]_i$ fluctuations; BDNF increased activation of the large sEPSCs in the tonic neurons and had little to no effect on the delay neurons or $[Ca2+]_i$ fluctuations. However, these data collectively suggest chronic BDNF may have reduced excitability in the delay and tonic SDH neurons, and this may provide a physiological basis for the depressive effect of chronic BDNF on the $[Ca2+]_i$ fluctuations. On the contrary, the 'silent' neurons are predicted to have responded to chronic BDNF with $[Ca2+]_i$ fluctuations of greater amplitude, total area, frequency, and presumably activation. Our working model (**Fig 6**, bottom) posits that under naïve conditions many delay and tonic SDH neurons in organotypic spinal cord cultures are generally in an active state, with some gap junction coupling with neighboring neurons. Long-term exposure to BDNF causes a homeostatic shift that pushes the SDH into a dampened state marked by synchronous, low-level activity spread across the network via increased gap junction coupling. This synchronous activity in turn mitigates the BDNF-activated 'silent' neurons.

Parameter	Delay neuron Large sEPSCs	Tonic neuron Large sEPSCs	SDH neuron $[Ca^{2+}]_i$ fluctuations	Silent SDH neuron $[Ca^{2+}]_i$ fluctuations
Amplitude	No effect ↔	Significant ↓	Significant ↓	Predicted ↑
Area under the curve	Significant ↓	Significant ↓	Significant ↓	Predicted ↑
Frequency	Significant ↑	Significant ↑	No effect ↔	Predicted ↑
Activation kinetics	No effect ↔	Significant ↑	No effect ↔	Predicted ↑

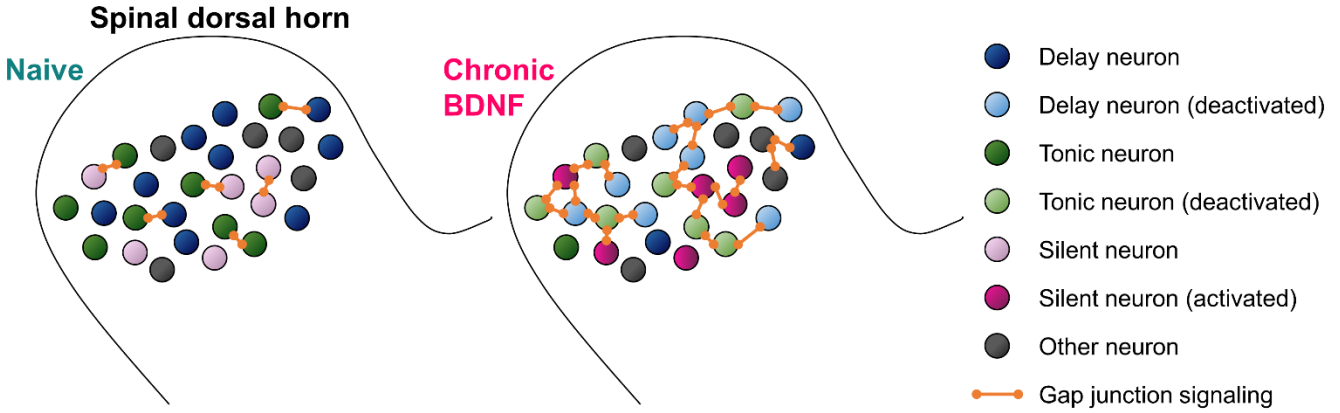

Figure 6. Working model summarizing the effects of chronic BDNF on SDH neurons in this study.

Several types of oscillatory and/or rhythmic bursting activity have been previously observed in spinal cord organotypic cultures (28,29) and in *ex vivo* slice preparations (23,30–32). Synchronous activation of groups of spinal nociceptive neurons might contribute to the 'electric shock'-like sensations experienced by some neuropathic pain patients (33). We hypothesize that $[Ca2+]_i$ fluctuations leading to synchronous network activity may be attributed to the "shooting pains" that chronic pain patients may experience. In particular, "shooting pain" is very commonly experienced by patients with radicular lower back pain (sciatica) or trigeminal neuralgia. In these patients, stimulus movement elicits so-called "traveling waves" in which neural activity sweeps across the body-part representation in somatosensory maps (34). The mechanisms of this have been attributed in part to Ca^{2+} waves and gap junctions (34,35). Therefore, given the properties of the $[Ca2+]_i$ fluctuations we have identified, they would make a good candidate for the neural substrate of shooting pain. In a cohort of chemotherapy-induced peripheral neuropathy (CIPN) patients, some of whom reported shooting or burning pain in the hands or feet, serum nerve growth factor (NGF) levels were much higher compared with patients with painless or absent CIPN (36). Therefore, there is a precedent for the correlation of neurotrophic factors related to BDNF to the incidence of shooting pain. Indeed it has been shown that NGF regulates the expression of BDNF (37). It is has also been demonstrated that BDNF overexpression induces spasticity in rodent models of spinal cord injury,

342 which may also explain the effect of BDNF on influencing network excitability in the dorsal horn (38). With
343 regards to the involvement of the dorsal horn in shooting pain, it has been shown that dorsal root entry
344 zone lesioning (DREZotomy) successfully reduces shooting pain caused by brachial plexus root avulsion
345 (BPRA) (39). Also, in one patient with shooting pain caused by osteoid osteoma, a partial laminectomy
346 was able to significantly relieve pain symptoms (40). Ideally however, more experiments using human *ex*
347 *vivo* tissue are needed to determine whether these particular $[Ca2+]_i$ fluctuations correlate with shooting
348 pain in patients.
349
350
351 **Materials and Methods**
352 *Defined-medium organotypic cultures of spinal cord slices*
353 Spinal cords were isolated from embryonic (E13-14) rats and transverse slices (300 ± 25 µm) were
354 cultured using the roller-tube technique (20,41). Since tissue is obtained from embryos, sex could not be
355 determined. Serum-free conditions were established after 5 days *in vitro.* Medium was exchanged with
356 freshly prepared medium every 3-4 days. Slices were treated after 15-21 days *in vitro* for a period of 5-6
357 days with 50-200 ng/ml in serum-free medium as described previously (20). Age-matched, untreated
358 DMOTC slices served as controls.
359
360 *Calcium imaging*
361 Each organotypic slice was incubated for 1 h prior to imaging with the fluorescent Ca^{2+}-indicator dye Fluo-
362 4-AM (Molecular Probes, Invitrogen, Carlsbad, CA, USA). The conditions for incubating the dye were
363 standardized across different slices to avoid uneven dye loading. After dye loading, the slice was
364 transferred to a recording chamber and superfused with external solution containing (in mM): 131 NaCl,
365 2.5 KCl, 1.2 NaH_2PO_4, 1.3 $MgSO_4$, 26 $NaHCO_3$, 25 D-glucose, and 2.5 $CaCl_2$ (20ºC, flow rate 4 ml/min).
366 Regions of interest (ROI) corresponding to individual cell bodies of neurons were identified based on
367 morphology and size. Changes in Ca^{2+}-fluorescence intensity evoked by a high K^+ solution (20, 35, or 50
368 mM, 90 s application)or other pharmacological agents, were measured in dorsal horn neurons with a
369 confocal microscope equipped with an argon (488 nm) laser and filters (20x XLUMPlanF1-NA-0.95
370 objective; Olympus FV300, Markham, Ontario, Canada). Full frame images (512 x 512 pixels) in a fixed
371 xy plane were acquired at a scanning time of 0.8-1.08 s/frame (42). In some experiments, images were
372 cropped to accommodate faster scan rates. Selected regions of interest were drawn around distinct cell
373 bodies and fluorescence intensity traces were generated with FluoView v.4.3 (Olympus).
374
375 *Electrophysiology*

Whole cell patch-clamp recordings were obtained from neurons in organotypic slice cultures under infrared differential interference contrast optics. Neurons selected for recording were located 250–800 µm from the dorsal edge of the cultures in an area presumed to reflect the *substantia gelatinosa* and up to a depth of 100 µm from the surface. Neurons were categorized according to their firing pattern in response to depolarizing current commands as tonic, delay, phasic, irregular, or transient (27). Recordings were obtained with an NPI SEC-05LX amplifier (ALA Scientific Instruments, Westbury, NY, USA) in bridge balance or in discontinuous, single electrode, current or voltage-clamp mode. Neurons were sampled at 2k Hz for 180 seconds when measuring sEPSCs. For recording, slices were superfused at room temperature (~22°C) with 95% O2-5% CO2-saturated aCSF that contained (in mM) 127 NaCl, 2.5 KCl, 1.2 NaH2PO4, 26 NaHCO3, 1.3 MgSO4, 2.5 CaCl2, and 25 d-glucose, pH 7.4. Patch pipettes were pulled from thin-walled borosilicate glass (1.5/1.12 mm OD/ID; WPI, Sarasota, FL) to 5- to 10-MΩ resistances when filled with an internal solution containing (in mM) 130 potassium gluconate, 1 MgCl2, 2 CaCl2, 10 HEPES, 10 EGTA, 4 Mg-ATP, and 0.3 Na-GTP, pH 7.2, 290–300 mosM.

Drugs and chemicals

Unless otherwise stated, all chemicals were from Sigma (St. Louis, MO, USA). Fluo-4 AM dye was dissolved in a mixture of dimethyl sulfoxide (DMSO) and 20% pluronic acid (Invitrogen, Burlington, Ontario, Canada) to a 0.5 mM stock solution and kept frozen until used. The dye was thawed and sonicated thoroughly before incubating with a DMOTC slice. TTX was dissolved in distilled water as a 1 mM stock solution and stored at -20ºC until use. TTX was diluted to a final desired concentration of 1 µM in external recording solution on the day of the experiment. Strychnine was prepared in a similar manner to TTX, and bicuculline (Tocris, Ballwin, MO, USA) was dissolved in DMSO as a 10 mM stock solution. 6-cyano-7-nitroquinoxaline-2,3-dione (CNQX, Tocris), 2,3-dihydroxy-6-nitro-7-sulfamoyl-benzo[f]quinoxaline-2,3-dione (NBQX, Tocris) and N,N,H,-Trimethyl-5-[(tricyclo[3.3.1.13,7]dec-1-ylmethyl)amino]-1-pentanaminiumbromide hydrobromide (IEM-1460, Tocris) were prepared as 10 mM stocks dissolved in distilled water, and D(-)-2-Amino-5-phosphonopentanoic acid (D-AP5, Tocris) was prepared as 50 mM stocks dissolved in 30% 1 M NaOH. Riluzole was prepared as a 10 mM stock, kyneurinic acid and GABA as 1 M stocks, and nitrendipine as a 1 mM stock made up in distilled water. These drugs were used at a 1:1000 dilution prepared freshly with external recording solution immediately prior to the start of experiments.

Data analysis and statistical testing

Raw time-lapse calcium fluorescence intensity and whole-cell voltage-clamp recordings were analyzed using the Frequency-Independent Biological Signal Identification (FIBSI) program (21) written using the

Anaconda v2019.7.0.0 (Anaconda, Inc, Austin, TX) distribution of Python v3.5.2 and the NumPy and matplotlib.pyplot libraries. The FIBSI program incorporates the Ramer-Douglas-Peucker algorithm to detect significant waveforms against a time-dependent generated reference line using the least number of total points to represent said waveform, and provides quantitative measurements for each detected waveform. The calcium fluorescence traces were fit using a sliding median with a window size between 5-25 s, and peaks below the sliding median line were traced together to form the reference line. The voltage-clamp traces were fit using a sliding median with a window of 50 ms, and peaks above the sliding median were traced together to form the reference line. A custom Python script was used to match sEPSCs detected in filtered voltage-clamp recordings with the unfiltered recordings. The detected sEPSCs for each neuron were clustered based on their amplitude, charge transfer, and interevent interval using the partitioning around medoids function (default settings, manhattan distance used) in the cluster v2.1.0 package in R v4.0.2 (2020-06-22; R Core Team, The R Foundation for Statistical Computing, Vienna, Austria). Each neuron was clustered independently. The average silhouette width method was used to select the optimal number of clusters for each neuron. Clusters were graphed using the plotly v4.9.2.1 package with dependency on ggplot2. The FIBSI source code, custom Python matching script, and a tutorial for using FIBSI are available on a GitHub repository (https://github.com/rmcassidy/FIBSI_program).

Statistical analysis of the calcium fluctuations and sEPSCs were performed using Prism v8.2.1 (GraphPad Software, Inc, La Jolla, CA). The comparison between the proportion of 'silent' neurons in the naïve and BDNF treatment conditions was made using Fisher's exact test. The Brown-Forsythe and Welch ANOVA tests and Games-Howell post-hoc test (for $n > 50$) were used to compare the effects of BDNF when the calcium fluctuations from all neurons were grouped together. To control for differences in recording times, the means for each fluctuation parameter (amplitude, AUC, etc.) were calculated for each neuron (fluctuations <10% the maximal amplitude in each neuron were omitted to remove the effects of low-amplitude noise). The amplitude and AUC means were normalized across all neurons to permit direct comparisons. Normality was assessed using the D'Agostino & Pearson omnibus test, and nonparametric comparisons between group medians were made using the Kruskal-Wallis test and Dunn's post-hoc test. Two-way repeated measures ANOVAs and Sidak's post-hoc tests were used to compare the pre- and post-treatment effects of octanol on the calcium fluctuations. Adjacency matrixes for neurons imaged together from the same organotypic culture were constructed using Pearson correlation matrixes; the FIBSI-processed calcium fluctuation recordings were used as input. Next, the mean Pearson *r* coefficient for each neuron within a culture was calculated using the Fisher Z transformation (steps shown in Fig 3A). The mean Pearson *r* coefficients in the naïve and BDNF

conditions were not normally distributed, so the comparison between the two was made using a Mann-Whitney test. Comparisons between the pre- and post-treatment effects of octanol were first made using a Wilcoxon matched-pairs signed rank test, and then using a two-way repeated measures ANOVA and Sidak's post-hoc test. Paired t-tests were used for pharmacology experiments. Brown-Forsythe and Welch ANOVA tests and Games-Howell post-hoc test were used to compare the effects of BDNF on the sEPSC clusters. Statistical significant was set to $P < 0.05$ and all reported P values are two-tailed. Details for the statistical analyses can be found in Table 1.

Acknowledgements

We thank Edgar Walters for useful discussions. We thank Klaus Ballanyi and Araya Ruangkittisakul for use of and technical assistance with confocal imaging equipment.

Competing Interests

We have no competing interests to disclose.

References

1. Finnerup NB, Haroutounian S, Kamerman P, Baron R, Bennett DLH, Bouhassira D, et al. Neuropathic pain: an updated grading system for research and clinical practice. PAIN. 2016 Aug;157(8):1599–606.

2. Alles SRA, Smith PA. Etiology and Pharmacology of Neuropathic Pain. Pharmacol Rev. 2018;70(2):315–47.

3. Sandkuhler J. Models and mechanisms of hyperalgesia and allodynia. Physiol Rev. 2009 Apr;89:707–58.

4. Stemkowski PL, Smith PA. Sensory neurons, ion channels, inflammation and the onset of neuropathic pain. Can J Neurol Sci J Can Sci Neurol. 2012 Jul;39(4):416–35.

5. Abdulla FA, Smith PA. Axotomy- and autotomy-induced changes in the excitability of rat dorsal root ganglion neurons. J Neurophysiol. 2001 Feb;85:630–43.

6. Amir R, Michaelis M, Devor M. Membrane potential oscillations in dorsal root ganglion neurons: role in normal electrogenesis and neuropathic pain. J Neurosci Off J Soc Neurosci. 1999 Oct 1;19(19):8589–96.

7. Djouhri L, Smith T, Ahmeda A, Alotaibi M, Weng X. Hyperpolarization-activated cyclic nucleotide–gated channels contribute to spontaneous activity in L4 C-fiber nociceptors, but not Aβ-non-nociceptors, after axotomy of L5-spinal nerve in the rat in vivo. PAIN. 2018 Jul;159(7):1392–1402.

8. Djouhri L, Zeidan A, Abd El-Aleem SA, Smith T. Cutaneous Aβ-Non-nociceptive, but Not C-Nociceptive, Dorsal Root Ganglion Neurons Exhibit Spontaneous Activity in the Streptozotocin Rat Model of Painful Diabetic Neuropathy in vivo. Front Neurosci [Internet]. 2020 [cited 2020 Sep 15];14. Available from: https://www.frontiersin.org/articles/10.3389/fnins.2020.00530/full

9. Boakye PA, Rancic V, Whitlock KH, Simmons D, Longo FM, Ballanyi K, et al. Receptor dependence of BDNF actions in superficial dorsal horn: relation to central sensitization and actions of macrophage colony stimulating factor 1. J Neurophysiol. 2019 01;121(6):2308–22.

10. Coull JA, Beggs S, Boudreau D, Boivin D, Tsuda M, Inoue K, et al. BDNF from microglia causes the shift in neuronal anion gradient underlying neuropathic pain. Nature. 2005 Dec 15;438:1017–21.

11. Guan Z, Kuhn JA, Wang X, Colquitt B, Solorzano C, Vaman S, et al. Injured sensory neuron-derived CSF1 induces microglial proliferation and DAP12-dependent pain. Nat Neurosci. 2016 Jan;19(1):94–101.

12. Scholz J, Woolf CJ. The neuropathic pain triad: neurons, immune cells and glia. Nat Neurosci. 2007 Nov;10(11):1361–8.

13. Tsuda M, Shigemoto-Mogami Y, Koizumi S, Mizokoshi A, Kohsaka S, Salter MW, et al. P2X4 receptors induced in spinal microglia gate tactile allodynia after nerve injury. Nature. 2003 Aug 14;424:778–83.

14. Ulmann L, Hatcher JP, Hughes JP, Chaumont S, Green PJ, Conquet F, et al. Up-regulation of P2X4 receptors in spinal microglia after peripheral nerve injury mediates BDNF release and neuropathic pain. J Neurosci. 2008 Oct 29;28:11263–8.

15. Woolf CJ. Evidence for a central component of post-injury pain hypersensitivity. Nature. 1983;306:686–8.

16. Coull JA, Boudreau D, Bachand K, Prescott SA, Nault F, Sik A, et al. Trans-synaptic shift in anion gradient in spinal lamina I neurons as a mechanism of neuropathic pain. Nature. 2003 Aug 21;424:938–42.

17. Ferrini F, Perez-Sanchez J, Ferland S, Lorenzo L-E, Godin AG, Plasencia-Fernandez I, et al. Differential chloride homeostasis in the spinal dorsal horn locally shapes synaptic metaplasticity and modality-specific sensitization. Nat Commun. 2020 Dec;11(1):3935.

18. Lu VB, Biggs JE, Stebbing MJ, Balasubramanyan S, Todd KG, Lai AY, et al. Brain-derived neurotrophic factor drives the changes in excitatory synaptic transmission in the rat superficial dorsal horn that follow sciatic nerve injury. J Physiol. 2009 Mar 1;587:1013–32.

19. Biggs JE, Lu VB, Stebbing MJ, Balasubramanyan S, Smith PA. Is BDNF sufficient for information transfer between microglia and dorsal horn neurons during the onset of central sensitization? Mol Pain. 2010;6:44.

20. Lu VB, Ballanyi K, Colmers WF, Smith PA. Neuron type-specific effects of brain-derived neurotrophic factor in rat superficial dorsal horn and their relevance to “central sensitization.” J Physiol. 2007 Oct 15;584:543–63.

21. Cassidy RM, Bavencoffe AG, Lopez ER, Cheruvu SS, Walters ET, Uribe RA, et al. Frequency-independent biological signal identification (FIBSI): A free program that simplifies intensive analysis of non-stationary time series data. bioRxiv. 2020 Jun 11;2020.05.29.123042.

22. Smith PA. BDNF: no gain without pain? Neuroscience. 2014 Dec 26;283:107–23.

23. Asghar AUR, Cilia La Corte PF, LeBeau FEN, Al Dawoud M, Reilly SC, Buhl EH, et al. Oscillatory activity within rat substantia gelatinosa in vitro: a role for chemical and electrical neurotransmission. J Physiol. 2005 Jan 1;562(Pt 1):183–98.

24. Chapman RJ, La Corte PFC, Asghar AUR, King AE. Network-based activity induced by 4-aminopyridine in rat dorsal horn in vitro is mediated by both chemical and electrical synapses. J Physiol. 2009 Jun 1;587(Pt 11):2499–510.

25. Ochalski PAY, Frankenstein UN, Hertzberg EL, Nagy JI. Connexin-43 in rat spinal cord: localization in astrocytes and identification of heterotypic astro-oligodendrocytic gap junctions. Neuroscience. 1996 Dec 11;76(3):931–45.

26. Kay CWP, Ursu D, Sher E, King AE. The role of Cx36 and Cx43 in 4-aminopyridine-induced rhythmic activity in the spinal nociceptive dorsal horn: an electrophysiological study in vitro. Physiol Rep. 2016;4(14).

27. Lu VB, Colmers WF, Smith PA. Long-term actions of BDNF on inhibitory synaptic transmission in identified neurons of the rat substantia gelatinosa. J Neurophysiol. 2012 Jul;108(2):441–52.

28. Fabbro A, Pastore B, Nistri A, Ballerini L. Activity-independent intracellular Ca2+ oscillations are spontaneously generated by ventral spinal neurons during development in vitro. Cell Calcium. 2007 Apr;41(4):317–29.

29. Sibilla S, Fabbro A, Grandolfo M, D'Andrea P, Nistri A, Ballerini L. The patterns of spontaneous Ca2+ signals generated by ventral spinal neurons in vitro show time-dependent refinement. Eur J Neurosci. 2009 Apr;29(8):1543–59.

30. Bardoni R, Ghirri A, Zonta M, Betelli C, Vitale G, Ruggieri V, et al. Glutamate-mediated astrocyte-to-neuron signalling in the rat dorsal horn. J Physiol. 2010 Mar 1;588(Pt 5):831–46.

31. Li J, Baccei ML. Pacemaker Neurons within Newborn Spinal Pain Circuits. J Neurosci. 2011 Jun 15;31(24):9010–22.

32. Ruscheweyh R, Sandkühler J. Long-range oscillatory Ca2+ waves in rat spinal dorsal horn. Eur J Neurosci. 2005 Oct;22(8):1967–76.

33. Baron R, Binder A, Wasner G. Neuropathic pain: diagnosis, pathophysiological mechanisms, and treatment. Lancet Neurol. 2010 Aug;9(8):807–19.

34. Defrin R, Brill S, Goor-Arieh I, Wood I, Devor M. "Shooting pain" in lumbar radiculopathy and trigeminal neuralgia, and ideas concerning its neural substrates. Pain. 2020;161(2):308–18.

35. Hanani M. Intercellular communication in sensory ganglia by purinergic receptors and gap junctions: implications for chronic pain. Brain Res. 2012 Dec 3;1487:183–91.

36. Velasco R, Navarro X, Gil-Gil M, Herrando-Grabulosa M, Calls A, Bruna J. Neuropathic Pain and Nerve Growth Factor in Chemotherapy-Induced Peripheral Neuropathy: Prospective Clinical-Pathological Study. J Pain Symptom Manage. 2017;54(6):815–25.

37. Pezet S, McMahon SB. Neurotrophins: mediators and modulators of pain. Annu Rev Neurosci. 2006;29:507–38.

38. Fouad K, Bennett DJ, Vavrek R, Blesch A. Long-Term Viral Brain-Derived Neurotrophic Factor Delivery Promotes Spasticity in Rats with a Cervical Spinal Cord Hemisection. Front Neurol [Internet]. 2013 Nov 19 [cited 2020 Jul 21];4. Available from: https://www.ncbi.nlm.nih.gov/pmc/articles/PMC3832889/

39. Yanagisawa T, Fukuma R, Seymour B, Hosomi K, Kishima H, Shimizu T, et al. MEG-BMI to Control Phantom Limb Pain. Neurol Med Chir (Tokyo). 2018 Aug 15;58(8):327–33.

40. Sarmiento JM, Chan JL, Cohen JD, Mukherjee D, Chu RM. L5 Osteoid Osteoma Treated with Partial Laminectomy and Cement Augmentation. Cureus. 2019 Mar 12;11(3):e4239.

41. Biggs JE, B. Lu, Kim HJ, Lai A, Todd KG, Ballanyi K, et al. Defined Medium Organotypic Cultures of Spinal Cord Put 'Pain in a Dish' #. In: T Isolated Central Nervous System Circuits. 2012. p. 405–36. (Neuromethods; vol. 73).

42. Ruangkittisakul A, Schwarzacher SW, Secchia L, Poon BY, Ma Y, Funk GD, et al. High sensitivity to neuromodulator-activated signaling pathways at physiological [K+] of confocally imaged

571 respiratory center neurons in on-line-calibrated newborn rat brainstem slices. J Neurosci Off J Soc
572 Neurosci. 2006 Nov 15;26(46):11870–80.

573

Supplemental Figures

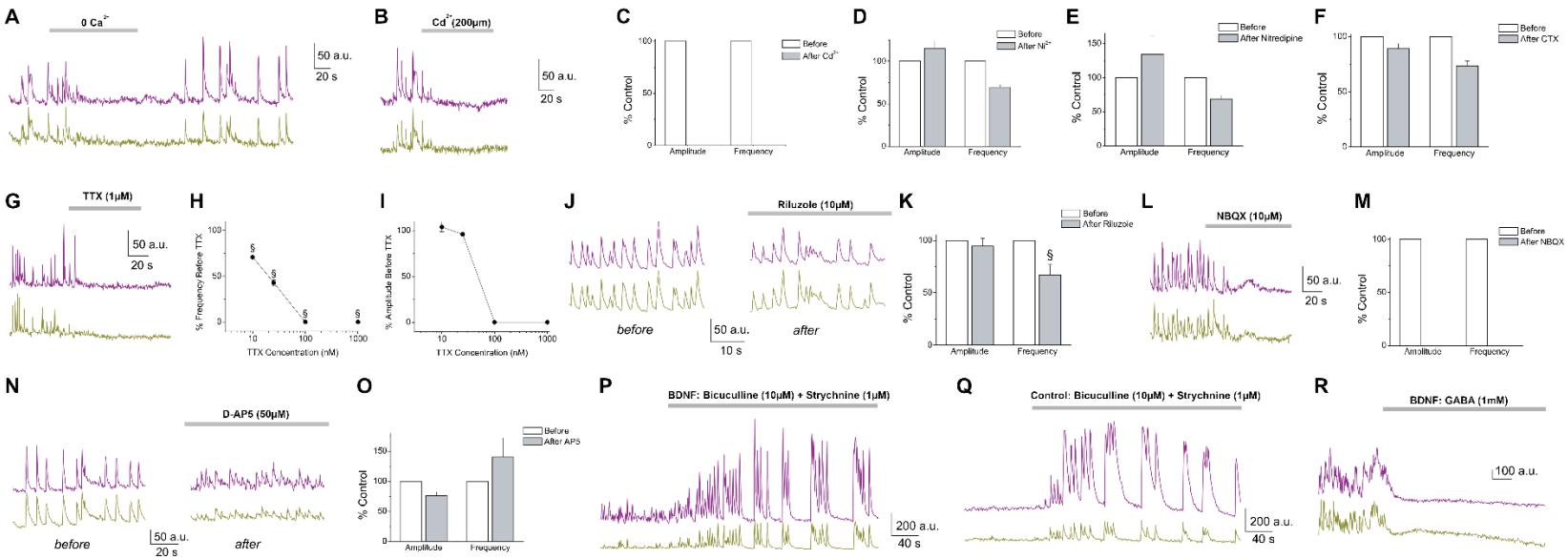

Supplementary Figure 1. Pharmacology of BDNF-induced Ca2+ fluctuations. Dependence of BDNF-induced Ca2+ fluctuations on extracellular Ca2+ entry through voltage-gated Ca2+ channels. **(A)** Perfusion of extracellular recording solution free of Ca2+ (0 Ca2+) marked by a thick grey line. Note the complete block of the fluctuations in recorded cells. **(B)** Addition of 200 µM Cd2+, marked by a thick grey line, abolished Ca2+ oscillations in a BDNF-treated slice. **(C)** Measurement of fluctuation amplitude and frequency before and after application of Cd2+. Values normalized to control values obtained before addition of Cd2+. **(D-F)** Effect of 100 µM Ni2+, 1 µM nitrendipine, and 100 nM ω-conotoxin GVIA on BDNF-induced fluctuation amplitude and frequency. Dependence of BDNF-induced Ca2+ fluctuations on TTX-sensitive voltage-gated Na+ current but not persistent Na+ current. **(G)** Addition of 1 µM TTX, marked by a thick grey line, abolished Ca2+ fluctuations in a BDNF-treated slice. **(H)** Concentration-inhibition curve for increasing concentrations of TTX on Ca2+ fluctuation frequency. **(I)** Concentration-inhibition curve for increasing concentrations of TTX on Ca2+ fluctuation amplitude. Error bars indicate standard error of the mean. For paired t-test, § = $p<0.001$. **(J)** Sample synchronous Ca2+ fluctuation traces from a BDNF-treated slice before (left) and after (right) application of 10 µM riluzole. **(K)** Effect of riluzole on average Ca2+

fluctuation amplitude and frequency. BDNF-induced Ca2+ fluctuations mediated by AMPA/kainate glutamate receptors. **(L)** Addition of 10 μM NBQX, marked by a thick grey line, abolished Ca2+ fluctuations in a BDNF-treated slice. **(M)** Measurement of fluctuation amplitude and frequency before and after application of NBQX. **(N)** Sample fluorescent Ca2+ traces from a BDNF-treated slice before (left) and after (right) application of 50 μM AP5. **(O)** Effect of AP5 on average Ca2+ fluctuation amplitude and frequency. Amplification of BDNF-induced Ca2+ oscillations by pharmacological removal of inhibition and suppression of oscillatory activity by GABA. **(P)** Addition of 10 μM bicuculline and 1 μM strychnine to a BDNF-treated slice produced robust fluctuations larger in amplitude but slower in frequency than the spontaneous Ca2+ fluctuations observed before antagonist application. **(Q)** Addition of 10 μM bicuculline and 1 μM strychnine to a control DMOTC slice produced similar robust fluctuations as those observed in P. **(R)** Application of 1 mM GABA, marked by a thick grey line, stopped BDNF-induced Ca2+ fluctuations. Average values represented. Error bars indicate standard error of the mean. For paired t-test, § = $p<0.001$, n=5-20 cells per condition.

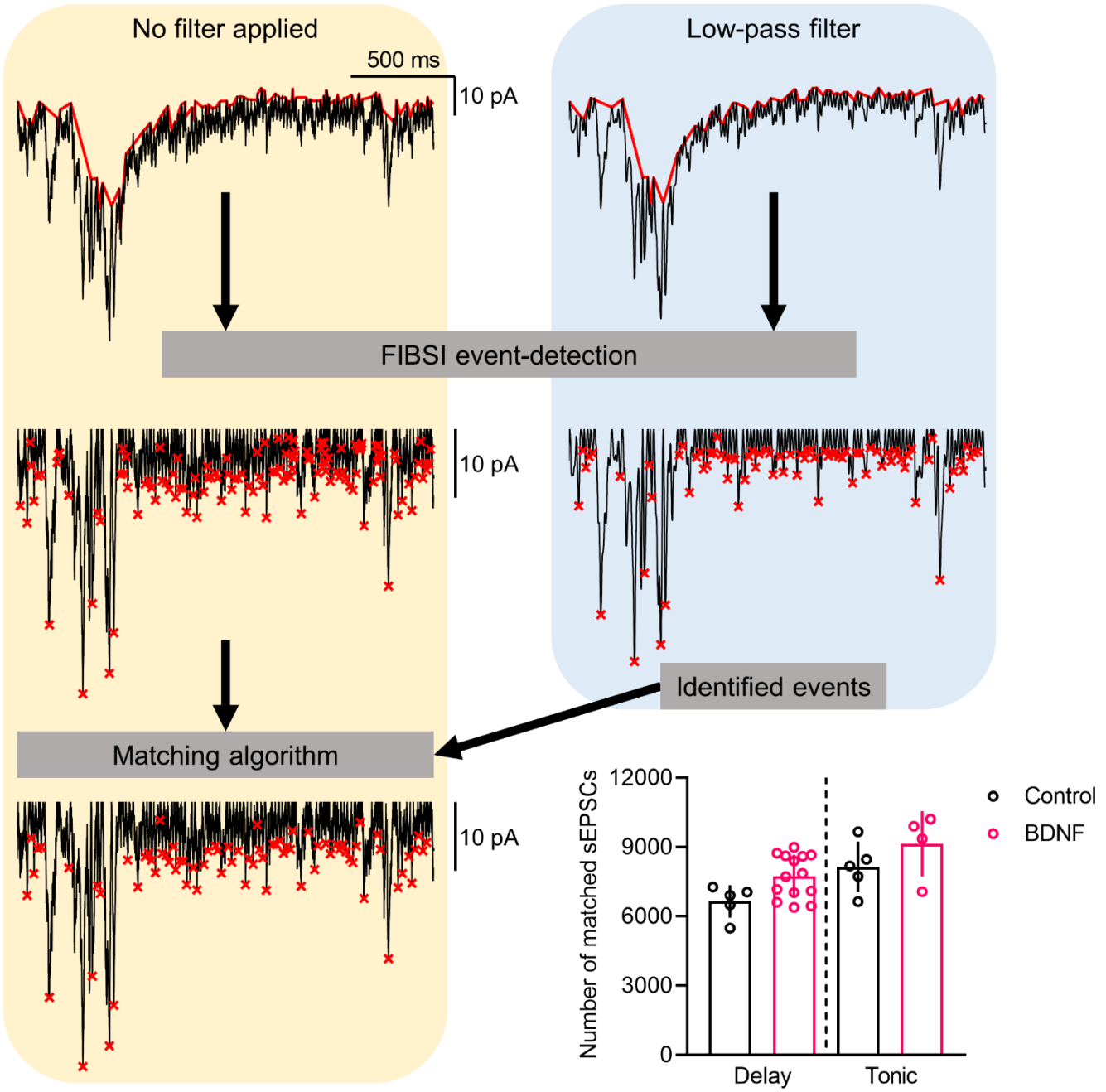

Supplementary Figure 2. Matching filtered spontaneous EPSCs detected by FIBSI with the raw recordings. All raw recordings were first analyzed by FIBSI without pre-processing filtering. All recordings were analyzed again following application of a low-pass filter with $\alpha = 0.05$. The output text files generated by FIBSI containing descriptive parameters (e.g., start time, peak time, amplitude, etc.) for each detected event were used as input to a custom Python script. The matching algorithm matched events detected in the filtered recordings with their corresponding events in the unfiltered recordings. Events were matched

607 based on peak event time and amplitude. Unmatched events were discarded from further analyses. The
608 total number of matched sEPSCs in the delay and tonic neurons are shown.

609

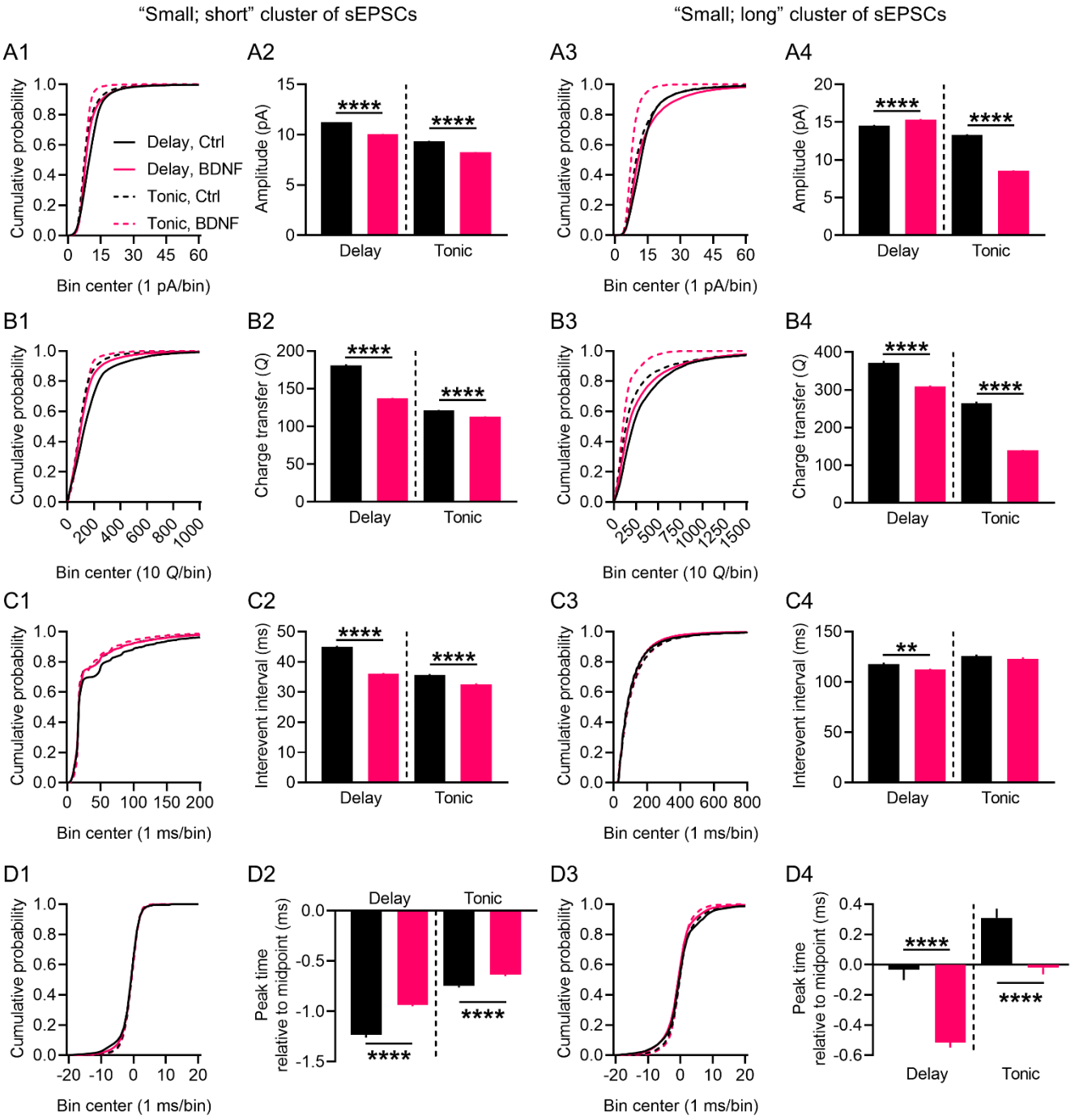

610

611 **Supplementary Figure 3.** Effects of BDNF on the two small clusters of spontaneous EPSCs in delay
612 and tonic-firing superficial dorsal horn neurons. Consistent, statistically significant effects of BDNF were

observed for the 'small; short" cluster of sEPSCs in the delay and tonic neurons; amplitudes were smaller **(A1-A2)**, charge transfer values were smaller **(B1-B2)**, within cluster interevent intervals were shorter **(C1-C2)**, and kinetics were slower **(D1-D2)**. Nuanced effects of BDNF were observed for the "small; long" cluster of sEPSCs in the two neuron types; sEPSC amplitudes were increased in delay neurons and decreased in tonic neurons **(A3-A4)** while charge transfer values were decreased in both types of neurons **(B3-B4)**. Interevent intervals in the delay neurons were significantly decreased, but not in the tonic neurons **(C3-C4)**. The sEPSC kinetics were significantly faster in the BDNF-treated delay and tonic neurons **(D3-D4)**. Small; short sEPSC cluster sample sizes: delay neurons control n = 20062, BDNF n = 69670; tonic neurons control n = 25235, BDNF n = 22086. Small; long sEPSC cluster sample sizes: delay neurons control n = 7638, BDNF n = 22391; tonic neurons control n = 7160, BDNF n = 5851. Comparisons between means in the control and BDNF conditions were made using Brown-Forsythe and Welch's ANOVA tests and Games-Howell post-hoc test. $^{**}P < 0.01$, $^{****}P < 0.0001$.